only in an optimally codoped minority component in samples such as $[K_{3.0}Tl_{4.5}C_{60}]$, where the majority phase has an expanded doped fcc structure. Fleming *et al.* (*18*) have shown that there is a linear correlation between the T_c of the alkali metal doped C_{60} and the unit cell parameter of the fcc phase, which is explained by band narrowing, resulting in an increased electronic density-of-states at the Fermi level, caused by decreased interactions between C_{60} molecules. Perhaps in part because of incomplete charge transfer from thallium, the transition temperatures observed here are either too low (K-Tl codopants) or too high (Rb-Tl codopants) to be consistent with the abovementioned correlation, assuming that the fcc unit cell parameter measured by x-ray diffraction corresponds to the superconducting fraction with enhanced critical temperatures. The bcc phase is unlikely to be the higher T_c superconducting phase in the thallium codoped samples, because of the absence of any positive correlation between the amount of this phase and the observed superconducting fraction, which is consistent with previous work on alkali metal doped C_{60} (*15, 17, 18*). The remaining observed crystalline phase in the K-Tl and Rb-Tl codoped samples is the bct phase, which is reported not to superconduct when doped only with alkali metals (*17*). However, since this phase is typically observable in small amounts in our superconducting K-Tl and Rb-Tl codoped samples and since our superconducting fractions are low, we cannot exclude the possibility that the enhanced critical temperatures result from a thallium and alkali metal codoped bct C_{60} phase. The answer to these questions regarding the structural nature of the superconducting phase will require the synthesis of thallium codoped superconductor samples with higher fractions of the enhanced critical temperature superconducting phase.

REFERENCES AND NOTES

1. A. F. Hebard *et al.*, *Nature* **350**, 600 (1991).
2. M. J. Rosseinsky *et al.*, *Phys. Rev. Lett.* 66, 2830 (1991).
3. K. Holczer *et al.*, *Science* **252**, 1154 (1991).
4. S. P. Kelty, C. C. Chen, C. M. Lieber, *Nature* **352**, 223 (1991).
5. K. Tanigaki *et al.*, *ibid.*, p. 222.
6. M. Kraus *et al.*, *Z. Phys. B*, in press.
7. W. Krätschmer, L. D. Lamb, K. Fostiropoulos, D. R. Huffman, *Nature* 347, 254 (1990).
8. M. Hansen, *Constitution of Binary Alloys* (McGraw-Hill, New York, 1958) p. 883.
9. R. Thümmel and W. Klemm, *Z. Anorg. Chem.* **376**, 44 (1970).
10. K. W. Blazey, A. M. Portis, J. G. Bednorz, *Solid State Commun.* **65**, 1153 (1988).
11. K. W. Blazey, in *Earlier and Recent Aspects of Superconductivity*, J. G. Bednorz and K. A. Müller, Eds. (Springer-Verlag, New York, 1990), p. 262.
12. F. J. Owens and Z. Iqbal, in *Studies of High Temperature Superconductors*, A. Narlikar, Ed. (Nova Publishers, New York, in press), vol. 9.
13. I. I. Khairullin, A. A. Zakhidov, P. K. Khabibullaev, Z. Iqbal, R. H. Baughman, *Synth. Metals* **33**, 243 (1989).
14. B. L. Ramakrishna, E.-W. Ong, Z. Iqbal, *J. Appl. Phys.* **64**, 5803 (1988).
15. P. W. Stephens *et al.*, *Nature* **351**, 632 (1991).
16. O. Zhou *et al.*, *ibid.*, p. 462.
17. R. M. Fleming *et al.*, *Nature* **352**, 701 (1991).
18. R. M. Fleming *et al.*, *ibid.*, p. 789.
19. *CRC Handbook of Chemistry and Physics*, D. R. Lide Ed. (CRC Press, Boca Raton, FL, ed. 71, 1990), pp. 8-19 and 12-1.
20. A. G. Lee, *The Chemistry of Thallium* (Elsevier, Amsterdam, 1971), pp. 245–246.
21. P. M. Allemand *et al.*, *J. Am. Chem. Soc.* **113**, 1050 (1991).

2 August 1991; accepted 1 October 1991

Liquids at Large Negative Pressures: Water at the Homogeneous Nucleation Limit

Q. ZHENG, D. J. DURBEN, G. H. WOLF, C. A. ANGELL

An isochoric cooling method for obtaining unprecedented tensions on liquids was used to determine the homogeneous nucleation limit for stretching of water at a variety of water densities. At densities in the range 0.55 to 0.68 gram per milliliter (g/ml), the data agree with the homogeneous nucleation temperatures measured by Skripov for superheated water at positive pressures. At densities between 0.68 and 0.93 g/ml, cavitation occurred only at negative pressures (that is, under tension). The cavitation tensions measured were in excellent agreement with those predicted by Fisher's 1948 vapor nucleation theory. A maximum tension of 140 megapascals (=1400 bars) was reached at 42°C, which lies on an extrapolation of the line of isobaric density maxima. At higher densities, cavitation of droplets that survived heterogeneous nucleation failed to occur at all unless provoked, at much lower temperatures, by freezing. This observation confirms the existence of a density maximum at 42°C and −140 megapascals and hence greatly strengthens the basis for Speedy's conjecture of a reentrant spinodal for water.

LIQUIDS UNDER TENSION (THAT IS, at negative pressure) are of interest because their behavior should be dominated by the intermolecular attractive forces rather than by the short-range repulsive (steric) forces, which, according to current theory (*1, 2*), control the structure and dynamics of liquids at normal and high pressures. However, because of the prevalence and efficiency of heterogeneous nuclei for vapor-phase nucleation, the negative-pressure region (metastability with respect to the vapor-liquid coexistence line on the one-component phase diagram) is much less easily investigated than the supercooled liquid region (metastability with respect to the liquid-crystal coexistence line). The particular case of water has, of course, been given the most attention. Despite experimental investigation since the 1840s (*3–8*) and the development of ingenious and sophisticated techniques (*4–8*), there have been no reports of controlled stretching of laboratory samples of water to negative pressures at all comparable to the theoretical limit, which is calculated as −140 MPa at 25°C from homogeneous nucleation theory (*9, 10*) or about −200 MPa at 35°C from spinodal breakdown theory (*11, 12*).

In 1950 Briggs succeeded in reaching −27.7 MPa with a rotating capillary technique (*4*), and Greenspan and Tschiegg (*5*) later reached −25 MPa with an acoustic technique. Henderson and Speedy (*8*) recently measured densities at −19 MPa with a spiral capillary version of Berthelot's original isochoric cooling technique (*3*). These pressure ranges were disappointing, but Roedder (*13*) found evidence for higher tensions in microscopic aqueous inclusions in certain minerals. He reported cases in which ice melted above 0°C, in one case reaching +6.5°C, which, from extrapolations of the melting line, implies a tension of at least 95 MPa in the inclusion. Combining this observation with Apfel and Smith's (*7*) demonstration that negative pressures in good agreement with the theoretical limit for homogeneous nucleation of bubbles of −1.7 MPa at 130°C could be generated in tiny droplets of ether sonically suspended in glycerine, we conjectured that large tensions close to the theoretical limit for bubble nucleation in water of −140 MPa could be obtainable if appropriate microsample techniques were used. Indeed, we recently demonstrated (*14*) that aqueous inclusions (actually saline solutions) found in microdispersed form in quartz crystals could sustain tensions up to 140 MPa. We have now used an inclusion synthesis technique

---

Department of Chemistry, Arizona State University, Tempe, AZ 85287.

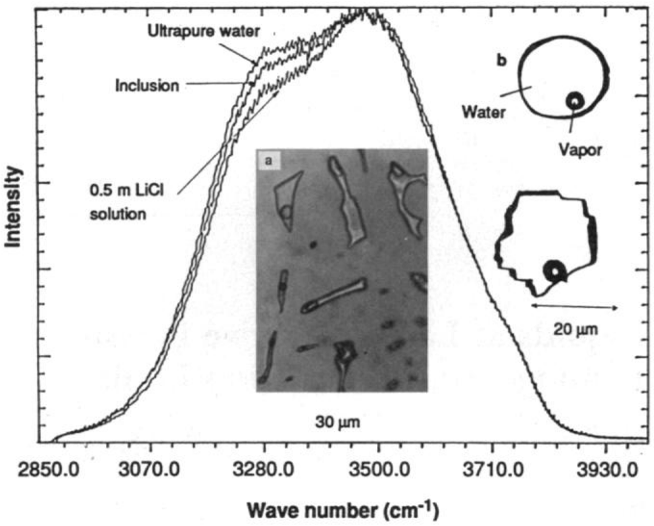

Fig. 1. Polarized (VV) Raman spectrum of microscopic inclusions of water in quartz matrices from this study compared with spectra of bulk water and a bulk 0.5 molal LiCl solution. (**Inset a**) Section of healed quartz crystal at ambient conditions showing inclusions (formed at 500°C and 4 GPa). (**Inset b**) Magnified examples of inclusions which, in this sample, have a T_d of 235°C and cavitate at −50 MPa.

developed by geochemists (*15*) to obtain results that we believe establish the static limits of metastability for water set by rapid homogeneous nucleation of cavities, in the temperature range extending from the critical temperature to below the freezing point.

To prepare samples, we cored high-quality crystals of quartz, calcite, and fluorite with a 3-mm coring drill and quench-fissured them in pure water at temperatures from 300° to 400°C. The fissured samples were sealed in Ag-Pd tubes containing a calculated quantity of ultrapure water and then autoclaved at a combination of pressure and temperature chosen to achieve the desired density of water within the inclusions. During autoclaving, the fissures heal and water is trapped in interstices. The shapes of the inclusions depend on the crystal symmetry group and the annealing time and conditions: with long annealing they form "negative crystals" (*16*).

Because annealing at high temperatures can lead to contamination of the water by alkali ions leached from defect sites in the crystal lattices (*16*), the purity of the samples was subject to confirmation. Comparisons of micro-Raman spectra of our inclusions with spectra of bulk water and dilute lithium chloride solutions were used to confirm that water purities were >99.2 mole percent in the quartz inclusions (see Fig. 1). Impurity levels in the calcite and fluorite inclusions were larger and reached ~2 mole percent salt in some fluorite samples (*17*).

As recovered at room temperature, all inclusions except those with the highest liquid densities contained bubbles produced by nucleation of the vapor phase during cooling (Fig. 1, insets a and b). To determine the relation of the liquid-state density to the vapor nucleation temperature, we polished the inclusion-containing crystals (perpendicular to their *c* axes) and mounted them in a microscope heating stage. Upon heating, the liquid phase in our inclusions expands at the expense of the vapor bubble and the pressure on the liquid is given by its vapor pressure along the equilibrium saturation line, T_{sat}. At a temperature T_d, the vapor bubble disappears, because the liquid phase has expanded to fill the entire inclusion void. On heating above T_d, the thermodynamic path of the inclusion must follow a liquid-state isochore, the density of which is located by T_d on the saturation line (see Fig. 2A). Likewise on cooling, the same liquid-state isochore will be followed until a bubble nucleates. A small deviation from an isochoric path arises as a result of the finite thermal expansivity and compliance of the quartz host (*18*).

The isochores displayed in Fig. 2A are based on the U.S. Bureau of Standards (HGK) equation of state (*19*) of water (a multiparameter fitting equation derived from high-precision data at pressures above the equilibrium vapor saturation line) and on extrapolations of this equation to pressures below the saturation line and into the negative pressure domain. Below the equilibrium saturation line, the liquid is thermodynamically metastable. The isochores ultimately terminate at the spinodal line, which signifies the limit of metastability, due to a mechanical instability, of the liquid phase. The spinodal line originates at the critical point and is determined from the equation of state by the condition $(\partial P/\partial V)_T = 0$.

Because the spinodal is determined by extrapolation, its exact location will depend on the form and parameters of the equation of state (EoS). The spinodal of the HGK equation is supported over a wide temperature range by the simpler Speedy equation (*12*), which is based on a series expansion of the liquid volume about the spinodal pressure limit P_s. The Speedy equation predicts a somewhat larger tensile strength, that is, limiting negative pressure, for water (see Fig. 2A) and is supported by the recent computer simulation study of Geiger *et al.* (*20*).

More important than the differences, however, is the fact that nearly all equations of state for water predict that the phase diagram has a feature that distinguishes it from that of nearly all other liquids, namely, the reversal of the spinodal pressure at low temperature. According to Speedy (*12*), this reversal coincides with, and is indeed thermodynamically required by, the intersection of the spinodal with the line of isobaric density maxima (the loci of points where the isobaric thermal expansivity changes sign). The return of the spinodal to positive pressures at temperatures below the equilibrium freezing line is the essential element of the Speedy interpretation of anomalies in supercooled water.

In no case is it expected that the spinodal boundary can be experimentally observed. Rather, the metastable state will be terminated by a homogeneous nucleation process that occurs when fluctuations of sufficient magnitude to establish thermodynamically viable embryos of the stable state become probable on the time scale of the observation (*9, 10, 21*). Thus the static limit to the stretched liquid state is determined by the pressure-dependent homogeneous bubble nucleation temperature. In our study, the liquid-state cavitation pressure (or tension) along a given isochore is determined by way of the EoS, by the measured temperature (*18*).

For the quartz hosts, all inclusions in a given sample exhibit the same bubble disappearance temperature T_d (±2°C) and hence follow the same isochore. Furthermore, for inclusions with T_d > 250°C (prepared at autoclave temperatures in excess of 400°C), the same cavitation temperature (within ±2°C) was observed for all inclusions in a given sample. However, for the higher density inclusions, T_d < 250°C, a scatter was observed in the cavitation temperatures of different inclusions (see Fig. 2B). Syntheses of these higher density samples required lower annealing temperatures (down to 300°C), and evidently sources of heterogeneous nucleation [possibly surfactant molecule clusters destroyed by annealing at the higher temperatures (*22*)] survived the inclusion formation process. For inclusions in the fluorite and calcite matrices, cavitation temperatures were always somewhat scattered, presumably also due to heterogeneous nucleation. Moreover, maximum cavitation tensions in the fluorite and calcite samples were also some 20 to 50% smaller than for the quartz samples; hence, no data from these cases are included in the figure.

For inclusions with liquid densities less than 0.68 g/ml (T_d > 315°C), cavitation in quartz matrices is observed at positive pressures, and the nucleation temperatures are in excellent accord with the homogeneous nucleation temperatures observed for superheated water by Skripov (*23*) (Fig. 2B inset). For higher densities, up to 0.93 g/ml, our maximum cavitation tensions fall on a natural extrapolation of the positive-pressure data to negative pressures and smoothly extend to the maximum observed tension of 140 MPa (HGK equation) or 147 MPa (Speedy equation). These results are in remarkable agreement with the predictions of Fisher's 1948 theory of homogeneous bubble nucleation in stretched water (*9*), which gives for the homogeneous nucleation pressure P_h

$$P_h = -\{(16\pi/3)\sigma^3/[kT\ln(nkTt/h) - \Delta f^*]\}^{1/2}$$

where σ is the surface tension of the liquid, n is the number of molecules in the sample, t is the time allowed for the nucleation event to be observed, Δf^* is the activation energy for motion of an individual liquid molecule past its neighbors into or away from the bubble surface, and k and h are Boltzmann's and Planck's constants, respectively (Fig. 2B, dashed line). In our calculations, Δf^* is taken to be the activation energy for viscosity and a waiting time, t, of 1 s was chosen. Note that P_h varies by less than 5% for observation times ranging between 10^{-3} and 10^3 s. We calculated the theoretical homogeneous nucleation line using values of σ at a specified temperature measured along the equilibrium saturation line (*24*). The values of P_h calculated from Fisher's equation are indistinguishable from those derived from a more recent development of homogeneous nucleation theory by Blander and Katz (*10*).

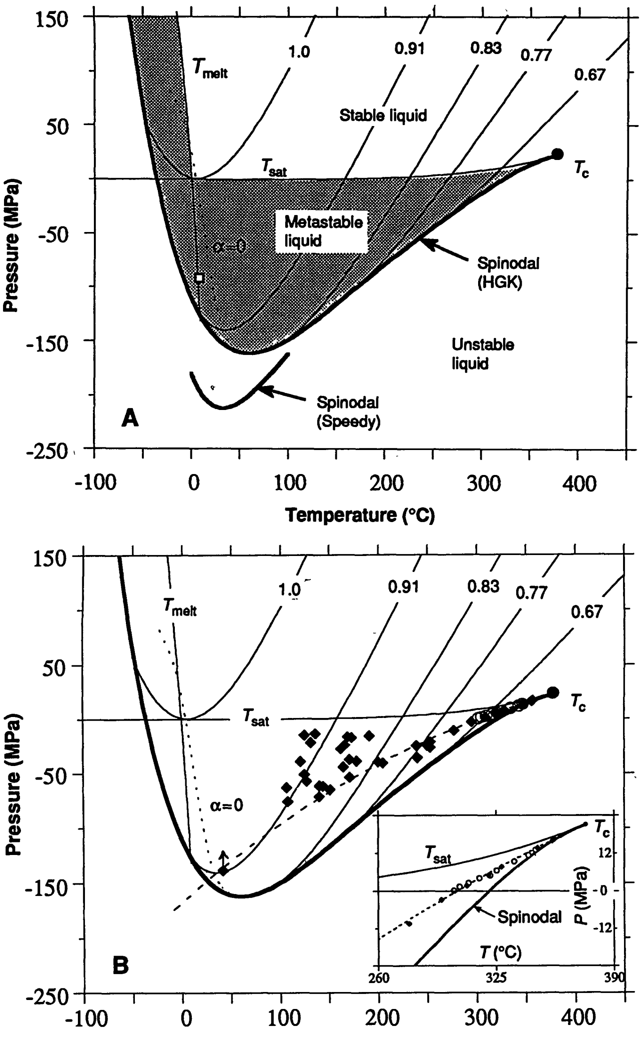

Fig. 2. (**A**) Isochores for water at different densities according to the HGK equation of state displayed against the equilibrium phase diagram. Isochores are extrapolated below the equilibrium liquid-vapor saturation line, T_{sat}, and into the negative pressure regime. Shaded area shows liquid states that are thermodynamically metastable but mechanically stable $[(\partial P/\partial V)_T < 0]$. The spinodal line, which originates at the critical point T_c, marks the limit of mechanical stability $[(\partial P/\partial V)_T = 0]$. Liquid states below this line are mechanically unstable $[(\partial P/\partial V)_T > 0]$ and cannot support any density fluctuations. The spinodal line for water changes slope at its intersection with the line of isobaric density maxima (locus of *T-P* points where the thermal expansivity is zero, indicated by the dotted line) and reenters the positive pressure regime at temperatures below the equilibrium freezing line, T_{melt}. The spinodal according to the EoS of Speedy indicates a larger limiting tension in the temperature range 0° to 190°C. The square at −95 MPa on the extrapolated melting line is the largest tension reported by Roedder (*13*) from inclusion studies of ice melting. (**B**) Temperatures and pressures of cavitation of microscopic inclusions of pure water in quartz crystals based on observed T_d and cavitation temperatures. For samples with T_d in excess of 250°C (density >0.8 g/ml), cavitation temperatures of inclusions within a given sample are scattered. The point at −140 MPa is the lowest temperature (greatest tension) at which cavitation was observed in this sample. The correction of this tension value due to the deviation from a true isochoric path is indicated by the small arrow (*18*). Other inclusions in this sample cavitated at higher temperatures and some others failed to cavitate at all, presumably because of a maximum in the *P-T* isochore indicated by the equation of state at about this temperature. Open circles in the main diagram and in the inset represent the superheating limit of water at positive pressures measured by Skripov (*23*). Our isochoric cavitation results at positive pressures are in excellent agreement with the isobaric superheating results of Skripov. The dashed line is calculated from Fisher's theory of homogeneous bubble nucleation in superheated and stretched water.

The success of the Fisher and Blander-Katz theory in the superheated regime (dashed line in the inset of Fig. 2B) has been recognized for some time, and its accord with our maximum cavitation tension line is strong evidence that our technique is indeed permitting us to explore the whole range of static mechanical stabilities for water. In view of this, it is of particular interest that in one of the samples with a large liquid-state density (0.91 g/ml and T_d = 160°C) inclusions surviving the heterogeneous nucleation regime behaved unusually. Some could be cooled to −40°C without cavitation, and one was observed in repeated runs to nucleate randomly in the range 40° to 47°C and occasionally not at all. In fact, no inclusion that survived cooling to 40°C ever nucleated bubbles during cooling to lower temperatures (although ice probably nucleated without being observable). This behavior is just that to be expected if the liquid isochore passes through a maximum tension as predicted by the EoS for the isochore in question. Indeed, the natural extrapolation of the line of experimental density maxima (*8*) predicts a value of about 43°C at −140 MPa. Thus the validity of the EoS far from its database is established at least to good approximation. But in this case the validity of the reentrant spinodal is also established because the EoS leaves no room for other behavior. This is an important inference because the reentrant spinodal conjecture (*12*) provides a detailed explanation of the extraordinary behavior of supercooled water at ordinary pressures (*25*). The occurrence of the tension maximum [previously observed in lower tension experiments (*8*)] should, of course, be confirmed by some direct means, for example, by an internal pressure probe (analogous to ruby chips in diamond anvil high-pressure cells), which presumably could be introduced into our inclusions by some exsolution process.

Water is one of the few substances that exhibit a density maximum, and hence reentrant spinodals will be uncommon. However, the gap between the homogeneous nucleation temperature and the spinodal will be common to all liquids. For most cases this region can only be explored by dynamic measurements of short time scale. In viscous liquids, on the other hand, it should be dynamically accessible on much longer time scales because of the sluggish fluctuation growth and decay times. In many liquids near their glass transition temperatures, tensions of the order of gigapascals are theoretically possible and should be observable. In the meantime it is important to utilize the present advances to determine the extent of the negative-pressure domains for other liquids and to perform measurements of structural, dynamic, and thermodynamic properties of liquids within these domains.

REFERENCES AND NOTES

1. D. Chandler, J. D. Weeks, H. C. Andersen, *Science* **220**, 787 (1983).
2. B. J. Alder and T. E. Wainwright, *J. Chem. Phys.* **27**, 1208 (1957).
3. M. Berthelot, *Ann. Chem. (Ser. 3)* **30**, 232 (1850).
4. L. Briggs, *J. Appl. Phys.* **21**, 721 (1950).
5. M. Greenspan and C. Tschiegg, *J. Res. Natl. Bur. Stand. Sect. C* **71**, 299 (1967).
6. R. Apfel, *J. Acoust. Soc. Am.* **49**, 145 (1971).
7. ______ and M. Smith, *J. Appl. Phys.* **48**, 2077 (1977).
8. S. Henderson and R. J. Speedy, *J. Phys. E* **13**, 778 (1980); *J. Phys. Chem.* **91**, 778 (1980).
9. J. C. Fisher, *J. Appl. Phys.* **19**, 1063 (1948).
10. M. Blander and J. Katz, *Am. Inst. Chem. Eng. J.* **21**, 833 (1975).
11. D. H. Trevena, *Contemp. Phys.* **17**, 109 (1976); *Am. J. Phys.* **47**, 341 (1979); *Cavitation and Tension in Liquids* (Adam Hilger, Bristol, England, 1987); S. W. Benson and E. Gerjuoy, *J. Chem. Phys.* **17**, 914 (1949); A. Saul and W. Wagner, *J. Phys. Chem. Ref. Data* **18**, 1537 (1989).
12. R. J. Speedy, *J. Phys. Chem.* **86**, 982 (1982).
13. E. Roedder, *Science* **155**, 1413 (1967).
14. J. L. Green, D. J. Durben, G. H. Wolf, C. A. Angell, *ibid.* **249**, 649 (1990).
15. S. M. Sternar and R. J. Bodnar, *Geochim. Cosmochim. Acta* **48**, 2659 (1984).
16. M. Rovetta, personal communication.
17. The Raman spectra were obtained with a triple spectrometer (Instruments S.A. S3000) equipped with a multichannel diode array detector (Princeton Instruments IY-750). Raman scattering was excited with the 488-nm line of an Ar^+ laser that was focused to a small spot (~5 μm) in the inclusion. Power levels at the inclusion were less than 10 mW. The VV polarized Raman scattered light was collected in a 180° backscattering geometry. To minimize birefringence effects, we oriented the sample such that the laser beam and collection optical axis were collinear with the *c* axis of the quartz host.
18. From data on the expansivity and compressibility of quartz and the compressibility of water we can calculate that the largest pressure correction needed for the matrix compliance effect will be 13% (at the maximum tension) and it falls rapidly at higher temperature.
19. L. Haar, J. Gallagher, G. S. Kell, *National Bureau of Standards-National Research Council Steam Tables* (McGraw-Hill, New York, 1985). See also C. A. Angell, W. J. Sichina, M. Oguni, *J. Phys. Chem.* **86**, 998 (1982).
20. A. Geiger, P. Mausbach, J. Schnitker, in *Water and Aqueous Solutions*, G. W. Neilson and J. Enderby, Eds. (Adam Higler, Bristol, England 1986), pp. 15–30; A. Geiger, in *Correlations and Connectivity*, H. E. Stanley and N. Ostrowsky, Eds. (Kluwer Academic, Dordrecht, 1990), p. 198.
21. D. W. Oxtoby, *J. Chem. Phys.* **89**, 7521 (1988).
22. J. L. Katz, personal communication.
23. V. P. Skripov, in *Water and Steam*, J. Straub and K. Scheffler, Eds. (Pergamon, Elmsford, NY, 1980).
24. N. B. Vargaftik, B. N. Volkov, L. D. Voljak, *J. Phys. Chem. Ref. Data* **12**, 817 (1983).
25. C. A. Angell, *Annu. Rev. Phys. Chem.* **34**, 593 (1983).

26. This work was supported by the National Science Foundation (grants NSF-DMR CHE8304887 and NSF-EAR8657437) and the Shell Fellowship Foundation. We are grateful to J. Holloway for allowing us the use of his high-pressure annealing facility and for advice.

2 May 1991; accepted 8 August 1991

Ice Flexure Forced by Internal Wave Packets in the Arctic Ocean

PETER V. CZIPOTT, MURRAY D. LEVINE, CLAYTON A. PAULSON, DIMITRIS MENEMENLIS, DAVID M. FARMER, ROBIN G. WILLIAMS

Tiltmeters on the Arctic Ocean were used to measure flexure of the ice forced by an energetic packet of internal waves riding the crest of diurnal internal bores emanating from the Yermak Plateau, north of the Svalbard Archipelago. The waves forced an oscillatory excursion of 36 microradians in tilt of the ice, corresponding to an excursion of 16 micrometers per second in vertical velocity at the surface and of 3.5 millimeters in surface displacement. Strainmeters embedded in the ice measured an excursion of 3×10^{-7} in strain, consistent with ice flexure rather than compression. The measured tilt is consistent with direct measurements of excursions in horizontal current near the surface (12 centimeters per second) and in vertical displacement (36 meters) of the pycnocline 100 meters below the surface.

INTERNAL GRAVITY WAVES IN THE world's oceans are important in transporting momentum and energy both horizontally and vertically. The wave field is remarkably constant in space and time, permitting the formulation of a "universal" statistical description (*1*), yet the processes that generate and dissipate these waves are not well understood. However, internal waves in the Arctic Ocean appear to be more variable than waves in other oceans (*2*) and hence may allow study of specific mechanisms of wave growth, propagation, and decay. Measurement of ice tilt is a simple way to observe internal waves from the surface of the Arctic Ocean.

Internal waves generate large displacements of water deep in the ocean. Vertical displacements at the surface are orders of magnitude smaller and masked by noise from turbulence and wind waves on open seas. In most internal wave models, such surface displacements are ignored and a rigid-lid boundary condition is invoked in which the vertical displacement of the sea surface is set to zero (*3*). The ice cover of the Arctic Ocean suppresses surface wave noise and enables direct measurement of vertical displacements of the surface forced by internal waves.

In this report, we describe coherent measurements of ice tilt forced by internal waves in the Arctic Ocean. Observations were made at the oceanography ice camp of the Coordinated Eastern Arctic Experiment (CEAREX) as it drifted over the northern flank of the Yermak Plateau (*4*). Three electrolytic bubble level tiltmeters (*5*) (Fig. 1) were frozen to the surface of the ice in a triangular array. One axis of each meter pointed north and the other east. Three triaxial strainmeters (*6*), with one arm of each meter pointing north, formed another array. We also measured vertical velocity and temperature in the pycnocline using an acoustic Doppler current profiler (ADCP) (*7*) and temperature sensors (*8*) moored near the center of the tilt and strain arrays. Three additional temperature sensors at a depth of 99.5 m formed a triangular moored array. Horizontal water velocity near the surface was measured with a triangular array of acoustic transmitters and receivers (*9*) centered about 337 m to the south of the ADCP mooring.

An internal wave packet was observed passing the ice camp at 82.53°N, 8.58°E between 00 and 02 hours universal time coordinated (UTC) on 18 April 1989 (Fig. 2) (*10*). The wave forced a peak-to-peak ice tilt of 36 μrad (*11*) in a north-south (N-S) direction, in phase with the vertical component of seawater velocity in the pycnocline (*12*) extending from about 100 to 200 m in water 1800 m deep. The vertical velocity in the packet had a maximum excursion of 15 cm/s at a depth near 125 m. Water temperature also revealed vertical displacement in a

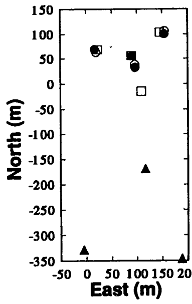

Fig. 1. Instrumentation layout at the CEAREX oceanography ice camp. Solid circles, tiltmeter array; open circles, strainmeter array; solid square, central mooring with ADCP and temperature meters; open squares, satellite moorings with temperature meters; solid triangles, vertices of the horizontal, path-averaging acoustic current meter. Coordinate orientation is aligned with true north for 18 April 1989.

P. V. Czipott, SQM Technology, Inc., Post Office Box 2225, La Jolla, CA 92038.
M. D. Levine and C. A. Paulson, College of Oceanography, Oregon State University, Oceanography Administration Building 104, Corvallis, OR 97331.
D. Menemenlis and D. M. Farmer, Institute of Ocean Sciences, Post Office Box 6000, Sidney, British Columbia, Canada V8L 4B2.
R. G. Williams, Department of Oceanography, U.S. Naval Academy, Annapolis, MD 21402.